HHS Public Access

Author manuscript

Int J Hyperthermia. Author manuscript; available in PMC 2020 November 05.

Published in final edited form as:

Int J Hyperthermia. 2012 ; 28(4): 320–336. doi:10.3109/02656736.2012.680173.

Mild hyperthermia with magnetic resonance-guided high-intensity focused ultrasound for applications in drug delivery

ARI PARTANEN[1,2,3], **PAVEL S. YARMOLENKO**[1,4], **ANTTI VIITALA**[5], **SUNIL APPANABOYINA**[6], **DIETER HAEMMERICH**[6], **ASHISH RANJAN**[1], **GENEVIEVE JACOBS**[1], **DAVID WOODS**[1], **JULIA ENHOLM**[5], **BRADFORD J. WOOD**[1], **MATTHEW R. DREHER**[1]

[1]Center for Interventional Oncology, Clinical Center, National Cancer Institute, National Institutes of Health, Bethesda, Maryland, USA, [2]Department of Physics, University of Helsinki, Helsinki, Finland, [3]Philips Healthcare, Cleveland, Ohio, USA, [4]Department of Biomedical Engineering, Duke University, Durham, North Carolina, USA, [5]Philips Medical Systems, Vantaa, Finland, [6]Department of Pediatrics, Medical University of South Carolina, Charleston, South Carolina, USA

Abstract

Purpose: Mild hyperthermia (40–45°C) is a proven adjuvant for radiotherapy and chemotherapy. Magnetic resonance guided high intensity focused ultrasound (MR-HIFU) can non-invasively heat solid tumours under image guidance. Low temperature-sensitive liposomes (LTSLs) release their drug cargo in response to heat (>40°C) and may improve drug delivery to solid tumours when combined with mild hyperthermia. The objective of this study was to develop and implement a clinically relevant MR-HIFU mild hyperthermia heating algorithm for combination with LTSLs.

Materials and methods: Sonications were performed with a clinical MR-HIFU platform in a phantom and rabbits bearing VX2 tumours (target = 4–16 mm). A binary control algorithm was used for real-time mild hyperthermia feedback control (target = 40–41°C). Drug delivery with LTSLs was measured with HPLC. Data were compared to simulation results and analysed for spatial targeting accuracy (offset), temperature accuracy (mean), homogeneity of heating (standard deviation (SD), T10 and T90), and thermal dose (CEM43).

Results: Sonications in a phantom resulted in better temperature control than in vivo. Sonications in VX2 tumours resulted in mean temperatures between 40.4°C and 41.3°C with a SD of 1.0–1.5°C (T10 = 41.7–43.7°C, T90 39.0–39.6°C), in agreement with simulations. 3D spatial offset was 0.1–3.2 mm in vitro and 0.6–4.8=mm in vivo. Combination of MR-HIFU hyperthermia and LTSLs demonstrated heterogeneous delivery to a partially heated VX2 tumour, as expected.

Conclusions: An MR-HIFU mild hyperthermia heating algorithm was developed, resulting in accurate and homogeneous heating within the targeted region in vitro and in vivo, which is suitable for applications in drug delivery.

Correspondence: Matthew R. Dreher, PhD, National Institutes of Health, 9000 Rockville Pike, Building 10, room 2N212, MSC 1182, Bethesda, MD 20892, USA. Tel: 301-402-8427. Fax: 301-496-9933. dreherm@cc.nih.gov.

Keywords

Drug delivery; liposome; mild hyperthermia; MR-HIFU; temperature sensitive liposome; thermotherapy

Introduction

Mild hyperthermia is a therapeutic technique in which cancerous tissue is heated above the body temperature to induce a physiological or biological effect but often not intended to directly produce substantial cell death. The goal is to obtain temperatures of 40°C to 45°C for time periods up to 1 h [1, 2]. In contrast, ablative hyperthermia is commonly greater than 55°C but for shorter durations of 20 s to 15 min [3]. Thermal dose (e.g. cumulative equivalent minutes at 43°C (CEM43)) has often been used to define the transition from mild hyperthermia to ablative hyperthermia (e.g. CEM43>240 may indicate ablative exposures [4, 5]). Hyperthermia treatments may result in both physiological (e.g. perfusion) and cellular (e.g. gene expression) changes that improve the therapeutic effectiveness when used in conjunction with chemotherapy or radiation therapy [1]. For example, several studies have shown that mild hyperthermia in combination with radiation and/or chemotherapy can improve response and survival [1, 2, 6, 7].

In addition to combination with traditional systemic chemotherapy and external beam radiotherapy, more recently hyperthermia has been combined with temperature responsive and non-responsive drug delivery systems in an effort to reduce systemic toxicity and improve overall efficacy. For non-responsive drug delivery systems, hyperthermia can improve the extravasation of nanoparticles [8, 9]. When hyperthermia is combined with temperature responsive drug delivery systems, the heat may also be used as a trigger to initiate an event such as drug release. Temperature responsive drug delivery systems include polymers (polyNIPAAm) [10], bio-polymers [11, 12], micelles [13] and liposomes [14]. One of the most promising temperature responsive drug delivery systems are temperature sensitive liposomes (TSLs) that release their contents in response to temperatures around the gel to liquid crystalline phase transition temperature of the lipid formulation [14–16].

Specifically, herein we use low temperature-sensitive liposomes (LTSLs), which contain a lysolecithin lipid and rapidly release encapsulated doxorubicin upon being heated to temperatures (40–42°C) within the mild hyperthermic range [17]. Previous studies combining LTSLs with local hyperthermia have demonstrated significant reduction in tumour volume in mouse tumour models compared with conventional free drug or non-thermally sensitive liposome therapy [17–20]. Furthermore, mild hyperthermia has been shown to assist drug delivery with liposomes by increasing vascular permeability, resulting in enhanced drug levels in solid tumours [8, 9] and may increase the sensitivity of cancer cells to chemotherapeutics [16].

The combination of regionally targeted, image-guided mild hyperthermia (40–45°C) and TSLs is an attractive and potentially clinically feasible strategy for augmenting delivery of drugs to solid tumours [21]. However, for this strategy of TSLs mild hyperthermia to realise its full potential in the clinic, hyperthermia applicators must provide accurate and

homogenous heating in a target region, often deep inside the body. Furthermore, the optimum temperature for most mild hyperthermia applications is in the 40–45°C range (T < 40°C causes limited effect, T>45°C may shut down tissue perfusion [22, 23]), and may require durations of 30–60 min [22], placing strict and challenging technical requirements on a hyperthermia applicator. Commonly used means for inducing hyperthermia include radiofrequency applicators [24–27], microwave applicators [28, 29], hot water baths [30], lasers [31, 32], and magnetic fluids [33, 34]. Despite some promising results, these devices and methods have drawbacks including highly invasive applicators, lack of spatial precision and temperature accuracy (such as hot or cool spots [25]), inability to achieve mild hyperthermia temperatures (40–45°C), and/or ability to only heat superficial tumours.

High intensity focused ultrasound (HIFU) utilises tightly focused ultrasonic waves, leading to absorption of energy and rapid, highly localised temperature elevations. HIFU represents an alternative to more widely used hyperthermia applicators. Although focused ultrasound was suggested for localised hyperthermia as early as the 1940s [35, 36], the lack of suitable image guidance and temperature control techniques prevented it from gaining widespread clinical adoption [37]. Due to its superior soft-tissue contrast, high spatial image resolution, and its ability to measure temperature changes, magnetic resonance imaging (MRI) is suitable for HIFU treatment planning and monitoring in real time (MR-HIFU). Temperature monitoring with MRI is commonly achieved with the water proton resonance frequency shift (PRFS) method [38], which utilises the linear dependence of PRFS on temperature change in the mild hyperthermic range in all non-adipose tissues [39, 40]. The PRFS method has been used to provide accurate and real-time thermometry free of interference from HIFU [41, 42]. Reliable magnetic drift correction could allow monitoring of long HIFU exposures using PRFS. Therefore, MR thermometry can be utilised to perform either operator adjustable or fully automated feedback control of the treatment [43–48] in order to improve the temperature accuracy and uniformity, and patient safety. Phased-array transducers in combination with appropriate driving electronics enable the creation of a desired focal pattern by making fast temporal displacement of the focus or the generation of multiple foci possible, thus significantly increasing the treated volume [5, 49–52]. Pre-clinical HIFU hyperthermia studies, both with and without image guidance, have also demonstrated enhanced release of drug and/or contrast agent from TSLs [47, 53–58], and improved gene expression [59,60]. These developments in both ultrasound applicators and MRI-based monitoring methods [39, 61–64] have made MR-HIFU mediated mild hyperthermia an attractive option as a non-invasive hyperthermia treatment modality, especially in combination with drug delivery.

The objectives of this study were to develop and implement a clinically relevant volumetric mild hyperthermia heating algorithm and to evaluate the ability to monitor and control heating in real time with MR-HIFU, using both tissue-mimicking phantoms and a rabbit VX2 tumour model. This mild hyperthermia technique was combined with LTSLs to demonstrate the potential of this combination strategy for image-guided local drug delivery.

Materials and methods

Tissue-mimicking gel phantom preparation

To develop and evaluate algorithms for MR-HIFU-mediated mild hyperthermia, tissue-mimicking gel phantoms were prepared using agarose (2 wt%, VWR International, Radnor, PA, USA) and 0.5–10 mm silica particles (2 wt%, Sigma-Aldrich, Schnelldorf, Germany) to provide scattering. These materials were added to distilled and degassed water, and the mixture was heated to 90°C with constant stirring for the agar to completely dissolve. After ~30 minutes at 90°C, the mixture was slowly cooled while stirring, to prevent settling of silica. Upon cooling down to 45°C, the gel was poured into a container (1 L) and allowed to solidify on ice. This procedure resulted in a gel phantom with a uniformly dispersed suspension of silica particles in a solid matrix of agarose [65]. While the acoustic cavitation threshold for this phantom is unknown, cavitation has not been observed in these phantoms at acoustic power levels reported herein.

Animal procedures and tumour model

All animal-related procedures were approved and carried out under an animal use protocol approved by the Animal Care and Use Committee. VX2 tumours in the superficial thigh muscle of New Zealand White rabbits (n = 10, ~2–3 kg body weight) were prepared as described by Ranjan et al. [66]. Briefly, VX2 was propagated in a donor rabbit, then inoculated into experimental rabbits as a single cell suspension under ultrasound guidance. Tumour growth was monitored with ultrasound for 2–3 weeks and MR-HIFU experiments were performed when the tumour was greater than 1 cm in any dimension.

One animal (animal 2 in Table I) was injected intravenously with LTSL (5 mg doxorubicin/kg, ThermoDox®, Celsion Corporation, USA) prior to its VX2 tumour being heated with MR-HIFU, and subsequently monitored for 4 h post-injection under anaesthesia, as previously described [66]. Following euthanasia, this animal's tumour was harvested and dissected into ten segments, and doxorubicin concentration was determined by HPLC [66] in each segment. At the end of the experiment, all animals were immediately euthanised by intravenous injection of Beuthanasia III (dose 0.2 mL/kg, pentobarbital sodium 390 mg/mL and phenytoin sodium 50 mg/mL).

In vitro phantom set-up

Prior to the experiments, the tissue-mimicking gel phantom was positioned on the treatment table, and acoustic coupling was achieved using degassed, distilled water.

In vivo experiment set-up

On the treatment day, the rabbits were anaesthetised with an intramuscular injection of ketamine and xylazine (28.6 mg/kg ketamine, 4.8 mg/kg xylazine). To ensure proper acoustic coupling, the tumour-bearing leg was carefully shaved and any remaining hair was removed using depilatory cream (Nair, Church & Dwight, Princeton, NJ, USA).

An animal was then positioned on top of the MR-HIFU treatment table. General anaesthesia was maintained using 1–3% isofluorane and oxygen through a nose mask. Acoustic coupling

was achieved by submerging the tumour-bearing thigh muscle in a degassed water bath directly above the transducer (Figure 1). Body temperature (rectal) and breathing rate were monitored using standard MR-compatible devices. An optical temperature probe (diameter 0.56 mm, Luxtron 3100, LumaSense Technologies, Santa Clara, CA, USA) was inserted in the thigh muscle near the tumour, and used for a baseline temperature for MR thermometry, prior to each sonication.

MR-HIFU platform

A clinical integrated MR-HIFU platform (Sonalleve 1.5T, Philips Medical Systems, Vantaa, Finland) was used both for sonications and MR guidance, using partly modified clinical software to suit small animal studies. The system was capable of delivering spatiotemporally controlled ultrasound energy, and consisted of a therapy control workstation, RF generators and control electronics, a treatment table that housed the electromechanical positioning system and a spherical-shell phased-array piezoelectric ultrasound transducer immersed in a sealed tank of degassed water, and a standard MR scanner (Achieva 1.5T, Philips Healthcare, Best, the Netherlands). The transducer could be mechanically translated along all three major axes as well as tilted, resulting in five degrees of freedom. The system also included a multi-element MR receive coil, which consisted of a single integrated element located around the acoustic window in the treatment table (below the animal) and another two elements that were embedded in curved and rigid plastic enclosure (above the animal). The coil elements were immobilised and not in direct contact with the animal.

A focused ultrasound beam was created using the 256-element (12 cm radius of curvature, 13 cm aperture) transducer, operated in continuous wave mode at 1.2 MHz. The ultrasound beam propagated vertically out of the sealed water tank and into the target through a thin (50 μm) circular Mylar membrane, with acoustic coupling provided by degassed water. The ellipsoid focal point produced by this transducer was approximately 1.6 mm × 1.6 mm × 10 mm (−6 dB), as measured along the ellipsoid axes using a needle hydrophone (Precision Acoustics, Dorchester, UK). Acoustic output power was calibrated using a radiation force technique (IEC-61161). In situ intensity (I_{spta}) at the focus was estimated from the total acoustic power, geometry of the transducer and the focal point, and an attenuation correction (based on muscle, absorption coefficient was assumed to be 0.5 dB $cm^{-1}MHz^{-1}$) to be 120 W/cm^2 for 7.5 W and 550 W/cm^2 for 35 W at a sonication depth of 15 mm in tissue [67].

The system-driving hardware and the workstation were located outside the MRI room. During therapy, in order to achieve desired outcome, the system allowed adjustments of the following parameters: size of the target region, output acoustic power, sonication duration, target temperature range, and ultra-sound frequency. The relative phases of ultrasound waves, separately produced by each element, were matched such that the individual waves interfered constructively at the desired focus. A heated volume of approximately 2 mm in diameter (~10 mm in length) resulted from a single focal point. Larger volumes were heated by rapid and sequential electronic steering of the ultrasound beam over a plane perpendicular to beam axis [5].

Treatment planning and MR thermometry

MRI was used to plan the therapy with 3D anatomical imaging as well as to monitor temperature rise with temperature-sensitive imaging during therapy, using the same sequences both in vitro and in vivo. Prior to therapy, proton density-weighted planning images were acquired as a 3D coronal stack, automatically transferred to the treatment workstation and used for ultrasound exposure planning. VX2 tumour was clearly visible in the thigh muscle as shown in Figure 2. The pulse sequence used for therapy planning was a 3D turbo spin echo (TSE) sequence with repetition time (TR) 1600 ms, time to echo (TE) 30 ms, matrix of 640 × 640, field of view (FOV) of 200 × 200 mm, slice thickness of 2 mm, stack of 80 slices, TSE factor 70, SENSE factor 2, bandwidth 585 Hz, coronal scan plane, and a total scan time of 5 min 47 s.

To monitor the induced temperature elevation during each sonication, multi-plane thermometry was performed during HIFU sonications using a dynamic fast field echo-echo planar imaging (FFEEPI) sequence. Two image slices were acquired; one coronal and one sagittal slice automatically positioned perpendicularly and parallel to the beam axis with the slices crossing at the centre of the target region (Figure 1). This imaging geometry allowed for simultaneous monitoring of the temperature evolution along and perpendicular to the beam axis. The temperature imaging sequence was a multishot RF-spoiled FFE-EPI with 7 k-space lines acquired per excitation. Identical imaging parameters were used for both slices: TR = 54 ms, TE = 30 ms, matrix of 144 × 144, FOV of 200 × 200 mm^2, slice thickness of 7 mm, flip angle 19°, bandwidth 252 Hz, and a 121-binomial water-selective excitation pulse. The resulting spatial resolution for both slices was 1.39 mm × 1.39 mm × 7.0 mm, with a total acquisition time of 2.5 s per dynamic. SNR-masked temperature maps were calculated in real time [5] from the resulting phase images using the PRFS (0.0094 ppm/°C) technique [38] and displayed as two-dimensional temperature maps (colour scale) overlaid on top of the magnitude images (greyscale) when $\Delta T > 2°C$. The obtained temperature maps were corrected for baseline drift by subtracting the average apparent temperature change of all voxels in a freehand-drawn reference region (coronal slice) near the ultrasound focus but outside of the target heated region (Figure 2). Temperature map mean noise level was calculated as an average (across all animals) of temperature standard deviation in the unheated region used for baseline drift correction.

Overview of mild hyperthermia volumetric feedback control algorithm

In this mild hyperthermia feedback implementation, the target region (known as a treatment cell) consists of concentric sonication subtrajectories, which together make up an entire trajectory. The trajectory consists of heat-up subtrajectories, temperature maintaining subtrajectories, and one wait subtrajectory during which the sonication power is 0 W. Trajectory geometry and size, number of subtrajectories, acoustic power, target temperature range, ultrasound frequency, and therapy duration are set by the user. The trajectory shape and size can be arbitrary.

Subtrajectories are heated for a specified duration using a combination of criteria, which can include temperature, thermal dose, temperature deviation, and SNR in the treatment cell or subtrajectory. Each criterion has its own limit(s); once reached, sonication can be stopped,

paused or switched to another subtrajectory (Figure 3A). In the initial heat-up phase, sonication is switched from a heat-up subtrajectory towards the next in a prescribed manner until all subtrajectories are sonicated once. After the sonication of the last heat-up subtrajectory is complete, sonication is switched to the wait subtrajectory. From the wait subtrajectory, sonication can be switched to any of the heat-maintaining subtrajectories, depending on the realised criteria. For each temperature map, the criteria of the maintaining subtrajectories are inspected and if any of the prescribed criteria have been realised, sonication is switched to the indicated subtrajectory (Figure 3A). If conditions for several heat maintaining subtrajectories are fulfilled at the same time, then the one that has prescribed priority is chosen to be sonicated first. From any of the heat maintaining subtrajectories, sonication is moved back to the wait subtrajectory once the action criteria of the maintaining subtrajec-tory have been realised.

Example action items (Figure 3):

- Heat-up: Sonication cycles through all heat-up subtrajectories.
- Wait: Once the criteria for the heat-up subtrajectories are met, heating is paused.
- Maintain: When temperature in one of the monitored subtrajectories drops below the lower limit, sonication resumes on that subtrajectory until the upper limit is reached.

Mild hyperthermia algorithm implementation

In this study, the design of the binary mild hyperthermia feedback control incorporated the volumetric heating approach and trajectory geometry described by Köhler et al. and elements of binary feedback control as described by Enholm et al. [5, 48].

Trajectory geometry and sonication timing.

The trajectory consisted of multiple concentric circles positioned in the plane perpendicular to the direction of HIFU propagation and centred on the axis of propagation. Sonication was started at the innermost subtrajectory and moved outward once the mean temperature limit had been reached in the current subtrajectory. Each circle consisted of several predetermined focal points that were regularly positioned by electronic steering along the circumference of the circle. The sonication time per point (50 ms) and the sonication order of the points (maximum distance between successive points) were chosen in order to produce a homogeneous spatial temperature distribution along each subtrajectory. The diameter of the treatment cell was adjusted by adding or removing subtrajectories (with different number of sonicated points along them), which had diameters of 4 mm (8 points), 8 mm (16 points), 12 mm (24 points) or 16 mm (32 points) [5]. Any given trajectory included all subtrajectories with a diameter equal to or smaller than the trajectory diameter. The sonication time at each subtrajectory was determined by the temperature limits.

Power and temperature limits.

The lower temperature limit was set to 40°C and the upper temperature limit was set to 41°C to be combined with LTSLs that exhibit release in this temperature range. Maximum temperature limit for the subtrajectories was 45°C in an effort to avoid reducing blood flow.

Duration of each hyperthermia treatment was 10 min. Before commencing the therapy sonications, an initial low-power test-sonication (acoustic power 10–15 W, $t \leq 20$ s) was performed in the target volume using a 4 mm treatment cell in order to determine the power setting for the therapy sonications, and to calibrate and confirm the correct location of heating. All heat-maintaining subtrajectories were sonicated at half the power used for the initial heat-up subtrajectories. Total acoustic power was constant within each subtrajectory but varied between subtrajectories to account for a decrease in energy deposition at the focus with larger electronic deflections [5]. In both animal and phantom experiments, an MR-compatible, passive cavitation detector integrated into the HIFU transducer was used to detect possible cavitation in real time during sonications.

Treatment cell placement and sonication process in vivo.

Treatment cell sizes were determined based on the size of the VX2 tumour by selecting the largest size that would fully fit inside the tumour in the coronal plane and inside the thigh muscle in the sagittal plane (4–12 mm diameter, ~2 × diameter in length). In two animals, the tumour was not accessible due to its close proximity to bone. In these cases, regions in muscle were targeted in order to obtain heating data from muscle and compare it with heating data from VX2 tumours. Between sonications, a fixed cool down period (5 min) was applied to ensure return to baseline temperature. This heat and cool cycle was then repeated to obtain additional data (2–7 treatment cycles/animal). In the phantom experiments, the temperature limits remained the same, but sonication duration was 30 min and cool-down time between sonications was 60 min (4–16 mm in diameter). Table I summarises the mild hyperthermia sonications performed in phantom and in each animal.

Example of mild hyperthermia feedback algorithm (Figure 3B):

1. Sonication starts at the innermost heat-up sub-trajectory, and is moved from one heat-up subtrajectory to the next once the mean upper temperature limit of 41°C is reached in the current subtrajectory. After the outermost heat-up subtrajectory has been completed, sonication is moved to the *wait subtrajectory*, which has 0 W acoustic power, and there is no sonication.
2. From the wait subtrajectory, the sonication is moved to a heat-maintaining subtrajectory if the mean temperature at that subtrajectory drops below 40°C. If this happens for several subtrajectories at the same time, the outermost of these subtrajectories is chosen for heating.
3. From the heat-maintaining subtrajectory, sonication is switched back to the wait subtrajectory when the mean temperature in that subtrajectory reaches 41°C, or when the maximum temperature in that subtrajectory exceeds 45°C.
4. Sonication is stopped when the maximum temperature limit in the entire trajectory is reached (50°C) or the treatment duration expired.

Simulations

The binary feedback algorithm (Figure 3) was modelled using the finite element method, which required measurement of the specific absorption rate (SAR). To gather these data,

each of the subtrajectories (4, 8 and 12 mm) of a 12 mm treatment cell were sonicated individually for 30 s at 100 W acoustic power and at a sonication depth of 6 cm in a tissue-mimicking phantom. SAR was calculated for each of the three subtrajectories from initial rate of temperature increase (bilinear approximation of the first 10 s). This calculation was performed for each voxel in the coronal MR image slice. The resulting SAR map was then interpolated to a smaller resolution (0.05 mm) used in the model. The finite element modelling was performed using Comsol 3.5A (Burlington, MA, USA) and used a triangular mesh of uniform size (0.05 mm) throughout the 10 × 10-cm axisymmetric model domain. Simulation time step varied between 0.1–1.0 s, depending on convergence of solution. The spatiotemporal temperature profile was then calculated using the Pennes' bioheat equation [68] where SAR (W/kg) was converted to the heat source term Q_{HIFU} (W/m^3):

$$\rho c\frac{\partial T}{\partial t} = \nabla \cdot k\nabla T + Q_{HIFU} - \rho_{bl}c_{bl}w_{bl}(T - T_{bl})$$

where T is the temperature; ρ, c, and k are tissue density, specific heat, and thermal conductivity, respectively; ρ_{bl}, c_{bl}, and w_{bl}, are blood density, specific heat, and perfusion respectively; T_{bl} is the arterial blood temperature; Q_{HIFU} is the external heat source term.

The values for tissue parameters in the equation above were adopted from earlier work [69]. Using this model, MR-HIFU mild hyperthermia was simulated for 10 min at three different perfusion levels (w_{bl}): (1) no perfusion, (2) 1 mL/mL/min (average perfusion for liver tumours) [70], and 2 mL/mL/min (high perfusion). Body temperature was set at 37°C for all simulations.

Hyperthermia treatment analysis

A total of 20 sonications were performed in phantoms and 39 sonications were performed in 10 rabbits. All sonications in rabbits that lasted the full duration of 10 min (n = 33) were analysed. Some sonications (n = 6) were aborted prematurely due to technical problems or animal movement (note: PRFS methods are sensitive to motion) and excluded from analysis. Parameters for analysed (completed) sonications are summarised in Table I. Data analysis was performed in Matlab 7.0 (MathWorks, Natick, MA, USA) and using in-house developed software package for IDL 6.1 (ITT Visual Information Solutions, Boulder, CO, USA).

The mean temperature, highest 10th percentile (T10), lowest 10th percentile (T90), and standard deviation (SD) in the target region were analysed from the coronal slice to assess temperature accuracy and uniformity. Targeting accuracy was assessed as a 3D spatial offset (3D distance) between the centroid of the mean temperature distribution and the center of the intended target region. Sonication efficiency was expressed as the ratio of volume heated over 40°C to the required energy (acoustic output power multiplied by actual sonication duration). Duration of sonication in each subtrajectory was analysed in order to assess the necessity of multiple subtrajectories. In addition, thermal dose accumulation in the target region was calculated according to the Sapareto-Dewey equation and reported using a unit of equivalent minutes at 43°C (CEM43) [71].

Heated volumes were assumed to be ellipsoids [5] for which the diameter, length, and volume ≥40°C were calculated. Heated region diameter and length were calculated as the mean distance with temperature ≥40°C (calculated from time-averaged data once T>39°C). A separate analysis was performed to assess B_0 magnetic field drift during therapy and its potential effect on apparent calculated temperature.

Statistical analysis

All regression and statistical analyses were performed using GraphPad Prism (version 5.0 for Windows, San Diego, CA, USA). Values are reported as mean standard deviation, unless stated otherwise. Spatial precision was determined by comparing 3D spatial offset values to the hypothetical offset of 0 using a one-sample *t*-test. Correlation analyses were performed using the Pearson correlation statistic. The relationship between sonication energy and treatment cell size was approximated with a linear regression. Sonication energy efficiency values were compared using one-way ANOVA across all treatment cell sizes. Pairwise comparisons with Tukey multiple comparison test were only reported when the ANOVA showed significant differences to protect against type I error. Sonications in muscle were not compared statistically due to insufficient sample size. Two-tailed p-values were obtained in all cases, with $p < 0.05$ being considered significant.

Results

Treatment planning and temperature imaging

High quality imaging will define the accuracy for any image-guided procedure – for MR-HIFU, MRI was used for treatment planning as well as temperature imaging, as shown in Figure 2. Quality and contrast of planning images were sufficient to identify the tumour (hyper-intense) from the surrounding normal tissue and then plan the treatment cell locations (Figures 2A and 2C). Hyperthermia treatment corresponded tightly with treatment cell location. Spatial accuracy in vitro was 0.1–3.2 mm and in vivo it was 0.6–4.8 mm with most of the error occurring in the beam axis direction. Temperature maps in vivo had a mean noise level of 0.6°C ± 0.2°C. Also, the partial magnetisation saturation introduced at the cross section of the two perpendicular slices did not adversely affect temperature imaging, consistent with previous reports [5]. This is important because the image plane intersection occurs at the HIFU focus.

Mean temperature over a 10-min sonication in vivo is shown in Figure 4A. The effect of magnetic drift on temperature measurements is clearly demonstrated in Figure 4B, with ~3°C change over 15 min of monitoring (9 body temperature in same time period was 0.2°C). Figure 4B shows an abrupt change in temperature due to animal motion at 500 s, highlighting the limitations of PRFS methods that use an image difference (current image phase – reference image phase) in organs or patients that may move.

Simulations

Figure 5A shows time-averaged spatial temperature distribution for a 12 mm treatment cell in silico during 10 min hyperthermia at normal perfusion (1 mL/mL/min). The simulated mean temperature >40°C spatially corresponds with the target cell boundary. Figures 5B and

5C show simulated mean temperature along the 4, 8 and 12 mm subtrajectories at two different perfusion levels: normal perfusion (1 mL/mL/min), and high perfusion (2 mL/mL/min). The centre of the treatment cell demonstrated slightly higher temperature overshoot during initial heat-up, likely due to heat diffusion from the outer trajectories. At high perfusion values (Figure 5C), the algorithm heated the innermost subtrajectory (4 mm) at 80, 120 and 170 s since its temperature dropped below the target range at these time points.

In vitro MR-HIFU mild hyperthermia

Sonications in tissue-mimicking phantoms are useful for characterising the performance of a hyperthermia algorithm as shown in Table II. Mean temperatures in the treatment cell correspond well with the target temperatures (target = T 40–41°C). Importantly, diameter of the heated volume (≥40°C) approximates the intended treatment cell diameter (difference < length of one voxel in the coronal plane), ensuring control over the heated area. Cavitation was not observed during any of the sonications in vitro.

In vivo MR-HIFU mild hyperthermia experiments

Volumetric sonications in vivo resulted in ellipsoid-shaped temperature elevations with the major axis in the direction of the HIFU beam propagation and a circular-symmetric cross section in the coronal plane (Figure 2), in good concordance with phantom experiments, and previously reported results [5, 48]. Mean temperature in the treatment cell rapidly reached the target temperature range (~0.14–0.75°C/s, faster for smaller treatment cells) as shown in Figure 6A. Upon completion of the sonication, temperature in the treatment cell returned to baseline levels over approximately 5 min. Agreement of temperature before and after sonication suggests that the magnetic drift correction was adequately applied. Cavitation was not observed during any of the sonications in vivo.

Larger treatment cells resulted in larger areas of hyperthermia as shown in Figure 6B and Figure 7. Diameter of the heated region over 40°C (lower temperature limit), closely corresponded to the treatment cell diameter, with a difference less than the length of a voxel (1.39 mm) in the coronal plane (see Table III). The heated region (T ≥ 40°C) length in the beam axis direction was found to be approximately 1.8 ± 0.6 times its diameter. There is a trend for larger treatment cells to increase temperature in the surrounding tissue more so than smaller cells. The difference between T10 and T90 was low (range = 2.5–4.1°C) indicating tight temperature control within the treatment volume.

Heating efficiency was significantly different across treatment cell sizes overall ($p < 0.0001$, one-way ANOVA, $n = 3–15$) as well as in all pair-wise comparisons ($p < 0.05$, Tukey). Furthermore, heating efficiency was positively correlated with treatment cell size both in the tumour ($p < 0.0001$, $r = 0.9812$, Pearson; Table IV) and in muscle ($p < 0.05$, $r = 0.9547$, Pearson; Table IV). The slope of a linear fit of efficiency versus cell size was 186 ± 8 c m^2/MJ ($p < 0.0001$, $r^2 = 0.9627$, linear regression) in the tumour and 280 ± 40 cm^2/MJ ($p = 0.0008$, $r^2 = 0.9114$, linear regression) in the muscle.

The algorithm selected the outermost subtrajectory for each treatment cell size to be heated most frequently (Table IV). For example, while heating the 12 mm treatment cell in a tumour, the algorithm selected the 12 mm subtrajectory 63%, 8 mm sub-trajectory 4% and 4

mm subtrajectory 12% of the treatment duration. The remaining 21% of treatment duration was spent in the wait subtrajectory. The algorithm's choice to heat inner subtrajectories of a 12 mm treatment cell is consistent with simulation results for high perfusion shown in Figure 5C, suggesting that homogeneity of heating may be improved through the use of multiple subtrajectories. Although tissue damage was not rigorously evaluated, no thermal damage was evident in the dissected tissue, consistent with the low thermal dose delivered (mean CEM43 ≤ 6.1, see Table III).

Drug delivery to a solid tumour

The ability of mild hyperthermia to improve drug delivery to a solid tumour with LTSLs was evaluated in one rabbit as shown in Figure 8. The treatment cell (4 mm) was placed within the tumour boundary (Figure 8A) and heated for a total of 30 min (four sonications, two of which completed a 10-min duration and were analysed; animal 2 in Table I). HPLC analysis of tumour segments upon dissection indicated varying levels of doxorubicin delivery to the tumour, as expected, since only a small volume of the tumour was heated (~2% tumour volume heated over 40°C, ~11% tumour volume heated over 39°C, Figure 8B). The ratio of the average drug concentration in the two segments with the highest drug concentration to that in the remaining segments was 3.7 ± 0.3 (Figure 8C).

Discussion

A binary feedback control algorithm for image-guided mild hyperthermia with MR-HIFU was developed for use with temperature-responsive drug delivery systems such as TSLs. Performance of this algorithm was evaluated in vitro and in vivo (in muscle and VX2 tumour), where this system demonstrated uniform heating of a region with accurate temperature control. This algorithm was implemented on a clinical MR-HIFU platform with future intention of translating the combination therapy of MR-HIFU and TSLs to the clinic.

Mild hyperthermia with MR-HIFU using binary feedback control has been demonstrated using approaches that are similar to what is reported herein [56, 57, 66, 72]. A binary feedback algorithm provides a simple and robust temperature control that does not require a priori knowledge of the tissue parameters. Alternative feedback control approaches for mild hyperthermia with MR-HIFU are limited in number but concentrate on the use of proportional-integral (PI) or proportional-integral-derivative (PID) feedback control [47, 60, 65, 73]. These methods rely in part on estimated tissue parameters, such as local perfusion and ultrasound absorption, to prescribe an applied power. These properties are known to be spatially heterogeneous and difficult to measure in tissue, potentially hampering the introduction of PID feedback style into clinical mild hyperthermia applications. However, alternative PID approaches (e.g., adaptive PID) may provide more robust temperature control that is less dependent on tissue parameters [73]. Comparative simplicity of the binary algorithm presented herein makes it an attractive candidate for clinical translation, as a similar feedback method has already been applied in clinical MR-HIFU ablations [74, 75].

The goal of triggering release from TSLs places specific demands on the implementation of mild hyperthermia in vivo. For example, an unanticipated high temperature may diminish local tissue perfusion [22, 23], which in turn may decrease drug delivery. Furthermore,

insufficient temperature elevations may not induce complete and/or rapid release from TSLs, again decreasing delivery. Therefore, a narrow temperature window exists for optimal drug delivery with TSLs, requiring a set of optimal performance criteria for the hyperthermia treatment including:(1) temperature accuracy, (2) spatial accuracy, (3) temporal control of heating, (4) tight temperature distribution within the treatment region, i.e. homogeneity, (5) conformal heating of the desired region, and (6) sufficient volume of heating. In the following sections, performance of the binary feedback algorithm for MR-HIFU will be addressed in context of these criteria.

Temperature and spatial accuracy

The binary control algorithm achieved mean temperatures (40.4–41.3°C, in vivo) that were prescribed by the target temperature range (40–41°C). The larger treatment cells tend to have a higher mean temperature most likely due to heat diffusion into the smaller subtrajectories during the heating of larger subtrajectories, especially during heat-up. Slight elevations above the upper temperature limit may be explained by a delay between the actual heating and acquisition of the temperature map. In other words, the temperature map represents the average temperature within the dynamic scan length (2.5 s) but the sonication may only be stopped at the end of each dynamic. This is an inherent problem tied to using an upper temperature limit for temperature control.

TSLs have an optimum temperature for release that depends on the lipid formulation [20, 76, 77]. For maximal drug delivery to occur, the target tissue should be heated to the optimal temperature for a duration long enough to achieve the desired level of drug delivery. Therefore, in the context of drug delivery with TSLs, the user should be able to prescribe the temperature range and treatment duration, as demonstrated herein.

In contrast to drug delivery with TSLs, thermal therapy is most often characterised with thermal dose (CEM43), which is based on an isoeffect, in most cases cell death. Although thermal dose required for cell death is tissue dependent [78], a thermal dose of 240 CEM43 is often used with MR-HIFU to indicate ablated tissue. In this study we achieved average thermal doses ≤ 6.1 CEM43 (range = 1.0–6.1 CEM43), suggesting no (or limited) thermal damage, given that thermal dose thresholds for tissue damage are typically much higher [78]. The binary control algorithm allowed for control over temperature and duration that in turn provided control over thermal dose. The benefits of adjuvant hyperthermia with radiation and/or chemotherapy are clearly demonstrated; however, sufficient thermal dose is positively correlated with outcome [79–84]. In addition to therapy with TSLs, temperature accuracy of the approach described herein suggests it may be used to deliver a specific deep interstitial thermal dose for applications in more traditional radiotherapy and chemotherapy clinical scenarios.

The spatial accuracy (3D spatial offset was 0.1–3.2 mm in vitro and 0.6–4.8 mm in vivo) appeared sufficient for targeting tumours that are often many cm in diameter. Spatial accuracy was lower in the beam axis direction, and may be improved upon by more sophisticated treatment planning that includes tissue specific modelling.

Temporal control of heating

The binary mild hyperthermia algorithm achieved rapid heat-up times (15–79 s, shorter for smaller treatment cells), in part because more power (2×) was used during heat-up subtrajectories than during the maintenance subtrajectories. Also, the outward moving concentric circle pattern takes advantage of the heat diffusion from inner subtrajectories to produce faster heat-up rates [5]. Total acoustic power was empirically selected based on the initial test sonication in order to obtain fast heat-up (<1 min) and stable maintenance while limiting the likelihood of mechanical effects (e.g. cavitation, acoustic radiation force). If too high a power was selected, greater temperature overshoot above the upper temperature limit might occur, while too low a power might never yield the desired temperature. These ultrasound exposures are similar to other reports that use MR-HIFU to achieve mild hyperthermia [56, 57, 66, 72]. Oscillations in temperature, that are apparent in Figure 6A, largely stay within our prescribed temperature limit of 40–41°C. Furthermore, computer simulations suggest that the frequency of these oscillations will depend on perfusion level (Figures 5B and 5C), and that the necessity of activation of inner trajectories increased with higher perfusion.

Homogeneity of heating

One of the major limitations in current hyperthermia applicators, such as radiofrequency applicators [24–27] and microwave applicators [28, 29], is the development of hot and cool spots both within and outside the prescribed treatment region. For example, simulations of radiofrequency heating indicate that maximum temperatures outside the treatment region may be greater than temperature maxima inside the prescribed treatment region by more than 1°C [25]. Within the treatment cell in vivo, MR-HIFU binary feedback algorithm performs quite well with an SD of 1.0–1.5°C and T10–T90 difference of 2.5–4.1°C. One drawback of the current algorithm is that for some sonications, the larger treatment cells have slightly (~0.5°C) higher temperature in the middle of the treatment cell (see Figures 5A, 6B, and 7). Possible explanations for this behaviour include higher acoustic intensities in smaller subtrajectories and heat diffusion from the outer subtrajectories (see simulation results, Figure 5). These higher temperatures in the centre may be ameliorated by decreasing the temperature limits and/or the maintenance power for the inner subtrajectories.

An additional challenge that could impact drug delivery with MR-HIFU and TSLs is near- and far-field heating outside of the prescribed treatment region, potentially resulting in poor spatial targeting of drug delivery. Near- and far-field heating results from HIFU energy deposition outside the focal plane and may be reduced by applying the optimal power, modifying the geometry of the focus, modifying the transducer design, or cooling the near-field.

Use of inner subtrajectories may make heating more homogeneous. This is suggested by the amount of time the algorithm spends heating inner subtrajectories, relative to overall treatment duration (Figure 5B and 5C and Table IV). A larger percentage of time spent heating inner subtrajectories implies that such heating was needed to maintain the 40–41°C target temperature. With a treatment cell size of 8 mm, the inner 4 mm subtrajectory was sonicated approximately 5% of the overall treatment duration, most of which was during

heat-up. In contrast, with a larger 12 mm treatment cell, 15–16% of the total treatment time was spent on the inner subtrajectories in muscle and tumour. For even larger treatment cells, such as 16 mm, the necessity to heat inner subtrajectories may be greater, especially in highly perfused organs/tissues. A direct comparison between heating performance using a single outer trajectory and multiple subtrajectories was not performed in vivo. However, the possible advantages of using multiple subtrajectories are suggested by simulations, where inner subtrajectories require heating with large treatment cells (12 mm cells, Figure 5C, high perfusion scenario), and by the required heating of inner subtrajectories 15–16% of the time in vivo (12 mm cells, Table IV). Finally, in cases with high perfusion or where heat diffusion is not sufficient to yield a uniform temperature distribution with larger trajectories, the need for multiple subtrajectories has been stressed by previously published work [85, 86]. These data suggest that the volumetric sonication approach employing concentric circular subtrajectories is beneficial for mild hyperthermia. Moreover, use of multiple concentric subtrajectories may aid in obtaining a uniform temperature distribution in the treatment cell, especially in highly perfused tumours (see simulation results, Figure 5).

Sonication efficiency

Larger treatment cells require more energy than smaller treatment cells to reach the target temperature range, but they offer the advantage of increasing the heated volume per unit of applied energy (Table III), as also seen in previous studies on thermal ablation [5, 48]. This increase in heating efficiency may allow total output power to be minimized, potentially increasing patient safety and equipment longevity. Compared to 4 mm, the efficiency was improved with greater treatment cell size, with 4- and 9-fold greater efficiency for 8 and 12 mm treatment cells, respectively. This could be explained by the decrease in surface area to volume ratio as the diameter of the target region increased. Since the heated volume largely dissipates energy through its surface, the amount of deposited energy increased relative to dissipated energy as the treatment cell size increased. The improvement in energy efficiency with increasing treatment cell size comes at a cost in terms of spatial accuracy of the temperature margins, as seen in Figure 6B. In clinical practice, drug delivery or thermal effects immediately adjacent to planned treatment volumes may be undesirable near critical anatomy. In such cases, smaller treatment cells might be required to provide sharp temperature gradients and ensure safety and predictability of heating. Alternatively, larger treatment cells may be used to heat a target lesion with a margin.

Image-guided hyperthermia

The implementation of binary feedback control for MR-HIFU employed imaging-based temperature feedback with a temporal resolution of 2.5 s. This provided limited over- and undershoot from the target temperature range, as shown by the data in Table III and Figure 6A. Temperature mapping may be further optimised by increasing spatial resolution, increasing the number of imaged slices, and using more than one slice for temperature feedback. However, these optimisations would most likely have a negative impact on the temporal resolution and/or SNR with the current MR coils. Image and temperature mapping quality may be improved with dedicated coil design for MR-HIFU applications. Furthermore, recent advances in temperature mapping including multi-baseline [87],

referenceless [88], and quantum coherence [89] may improve quality and control of mild hyperthermia treatment, potentially improving outcomes.

B_0 magnetic drift correction is often not required in MR-HIFU ablations where high temperatures are reached (>55°C) for short durations (~1 min), but drift correction is essential for mild hyperthermia with small ΔT and longer treatment times. The influence of magnetic drift affecting the phase, and therefore measured temperature, was clearly demonstrated in Figure 4. Over 15 min, magnetic drift typically resulted in apparent temperature changes between 0.5°C and 3.4°C. Similarly, motion also influences the phase and resulting temperature calculation with PRFS-based techniques. Additional techniques may be required, depending on the treatment location and desired spatial accuracy, to correct for motion or magnetic drift [90].

Future directions

In addition to improvements in the current implementation discussed above, future development of conformal large volume heating may aid clinical implementation of MR-HIFU hyperthermia. Ability to heat larger volumes may be useful for TSL drug delivery as well as radiosensitisation. Limitations of the current approach are clearly demonstrated in Figure 8, where the entire tumour volume was not heated, most likely leading to the expected nonuniform drug delivery to the tumour. The higher drug concentrations observed in two of the tumour segments likely correspond to the location of the heated volume (Figure 8). Heating the entire tumour by simultaneous sonication of multiple and/or larger treatment cells may improve homogeneity of drug delivery in this setting. It is probable that sufficient drug coverage of an entire tumour will lead to better therapy. A more in-depth analysis of an LTSL combined with this MR-HIFU mild hyperthermia algorithm has been reported elsewhere [66].

Despite the simplicity of concentric subtrajectories and binary control, the current approach cannot conform to any shape or volume, as many clinical applications may require. Similar to ablation approaches, multiple treatment cells may be arranged to cover a tumour [74] or a conformal treatment cell could be used to cover the entire target volume. The current implementation may not be adequate for heating highly heterogeneous regions, since this algorithm based feedback control on symmetric subtrajectories that spanned the entire target region. Voxel-wise temperature feedback may further improve conformability of heating. Although more complicated to implement, alternative feedback methods such as proportional, PI, or PID feedback may work well with voxel-wise conformal heating approaches.

Large volume heating with electronic steering of the HIFU focus alone is challenged by loss of acoustic intensity and formation of unwanted hot-spots with large electronic focal spot deflections. Alternative transducer designs may provide greater electronic deflection while retaining control over the focal spot shape. Mechanical steering alone is also ill-suited for large volume hyperthermia because motion of the transducer is slow compared to electronic steering and results in MR thermometry artefacts [47]. One potential solution to heat large volumes is to use a combination of electronic and mechanical steering of the HIFU focus. This approach is currently being explored.

Conclusion

This work demonstrated development and implementation of a binary mild hyperthermia feedback algorithm on a clinical MR-HIFU platform, resulting in accurate and homogeneous heating within the targeted region both in tissue-mimicking phantom and in a rabbit muscle and VX2 tumour. The temperature elevations corresponded spatially to the targeted locations with good spatiotemporal temperature stability and uniformity during long hyperthermia treatments (~10 min). This mild hyperthermia algorithm provides precise and non-invasive hyperthermia treatment, potentially benefiting clinical applications that require spatiotemporal control over heating of deep seated tumours, such as chemotherapeutic delivery with TSLs and radiosensitisation.

Acknowledgements

The authors thank Dr. Max Köhler, Jaakko Tölö, Matti Tillander, Ricky Long, and Dr. Sham Sokka of Philips Healthcare as well as Dr. Aradhana Venkatesan of NIH for their support and advice.

Declaration of interest: This research was supported by the Center for Interventional Oncology and Intramural Research Program of the National Institutes of Health (NIH), and through a Cooperative Research and Development Agreement (CRADA) with Philips Healthcare and Celsion Corporation. Ari Partanen, Antti Viitala, and Julia Enholm are paid employees of Philips Healthcare. The mention of commercial products, their source, or their use in connection with material reported herein is not to be construed as either an actual or implied endorsement of such products by the National Institutes of Health. The authors alone are responsible for the content and writing of the paper.

References

1. Viglianti BL, Stauffer P, Repasky E, Jones E, Vujaskovic Z, Dewhirst MW. Hyperthermia In: Hong W, Bast R Jr, Hait W, Kufe DW, Holland JF, Pollock RE, et al., editors. Holland Frei Cancer Medicine. Shelton, CT: Peoples Medical Publishing House-USA; 2010 pp 528–540.
2. Issels RD, Lindner LH, Verweij J, Wust P, Reichardt P, Schem BC, et al. Neo-adjuvant chemotherapy alone or with regional hyperthermia for localised high-risk soft-tissue sarcoma: A randomised phase 3 multicentre study. Lancet Oncol 2010;11:561–570. [PubMed: 20434400]
3. Wood BJ, Ramkaransingh JR, Fojo T, Walther MM, Libutti SK. Percutaneous tumor ablation with radiofrequency. Cancer 2002;94:443–451. [PubMed: 11900230]
4. Meshorer A, Prionas SD, Fajardo LF, Meyer JL, Hahn GM, Martinez AA. The effects of hyperthermia on normal mesenchymal tissues. Application of a histologic grading system. Arch Pathol Lab Med 1983;107:328–334. [PubMed: 6687797]
5. Köhler MO, Mougenot C, Quesson B, Enholm J, Le Bail B, Laurent C, et al. Volumetric HIFU ablation under 3D guidance of rapid MRI thermometry. Med Phys 2009;36:3521–3535. [PubMed: 19746786]
6. Falk MH, Issels RD. Hyperthermia in oncology. Int J Hyperthermia 2001;17:1–18. [PubMed: 11212876]
7. Wust P, Hildebrandt B, Sreenivasa G, Rau B, Gellermann J, Riess H, et al. Hyperthermia in combined treatment of cancer. Lancet Oncol 2002;3:487–497. [PubMed: 12147435]
8. Kong G, Braun RD, Dewhirst MW. Characterization of the effect of hyperthermia on nanoparticle extravasation from tumor vasculature. Cancer Res 2001;61:3027–3032. [PubMed: 11306483]
9. Kong G, Dewhirst MW. Hyperthermia and liposomes. Int J Hyperthermia 1999;15:345–370. [PubMed: 10519688]
10. Li W, Cai X, Kim C, Sun G, Zhang Y, Deng R, et al. Gold nanocages covered with thermally-responsive polymers for controlled release by high-intensity focused ultrasound. Nanoscale 2011;3:1724–1730. [PubMed: 21321760]

11. Meyer DE, Kong GA, Dewhirst MW, Zalutsky MR, Chilkoti A. Targeting a genetically engineered elastin-like polypeptide to solid tumors by local hyperthermia. Cancer Res 2001;61:1548–1554. [PubMed: 11245464]
12. Dreher MR, Liu W, Michelich CR, Dewhirst MW, Chilkoti A. Thermal cycling enhances the accumulation of a temperature-sensitive biopolymer in solid tumors. Cancer Res 2007;67:4418–4424. [PubMed: 17483356]
13. Park JS, Akiyama Y, Yamasaki Y, Kataoka K. Preparation and characterization of polyion complex micelles with a novel thermosensitive poly(2-isopropyl-2-oxazoline) shell via the complexation of oppositely charged block ionomers. Langmuir 2007;23:138–146. [PubMed: 17190496]
14. Yatvin MB, Weinstein JN, Dennis WH, Blumenthal R. Design of liposomes for enhanced local release of drugs by hyperthermia. Science 1978;202:1290–1293. [PubMed: 364652]
15. Weinstein JN, Magin RL, Yatvin MB, Zaharko DS. Liposomes and local hyperthermia: Selective delivery of methotrexate to heated tumors. Science 1979;204:188–191. [PubMed: 432641]
16. Landon CD, Park J-Y, Needham D, Dewhirst MW. Nanoscale drug delivery and hyperthermia: The materials design and preclinical and clinical testing of low temperature-sensitive liposomes used in combination with mild hyperthermia in the treatment of local cancer. Open Nanomed J 2011;3:38–64. [PubMed: 23807899]
17. Kong G, Anyarambhatla G, Petros WP, Braun RD, Colvin OM, Needham D, et al. Efficacy of liposomes and hyperthermia in a human tumor xenograft model: Importance of triggered drug release. Cancer Res 2000;60:6950–6957. [PubMed: 11156395]
18. Chelvi TP, Jain SK, Ralhan R. Hyperthermia-mediated targeted delivery of thermosensitive liposome-encapsulated melphalan in murine tumors. Oncol Res 1995;7:393–398. [PubMed: 8747602]
19. Yarmolenko PS, Zhao Y, Landon C, Spasojevic I, Yuan F, Needham D, et al. Comparative effects of thermosensitive doxorubicin-containing liposomes and hyperthermia in human and murine tumours. Int J Hyperthermia 2010;26:485–498. [PubMed: 20597627]
20. Needham D, Anyarambhatla G, Kong G, Dewhirst MW. A new temperature-sensitive liposome for use with mild hyper-thermia: Characterization and testing in a human tumor xenograft model. Cancer Res 2000;60:1197–1201. [PubMed: 10728674]
21. Wood BJ, Locklin JK, Viswanathan A, Kruecker J, Haemmerich D, Cebral J, et al. Technologies for guidance of radiofrequency ablation in the multimodality interventional suite of the future. J Vasc Interv Radiol 2007;18:9–24. [PubMed: 17296700]
22. Song CW. Effect of local hyperthermia on blood flow and microenvironment: A review. Cancer Res 1984;44:4721s–4730s. [PubMed: 6467226]
23. Bicher HI, Hetzel FW, Sandhu TS, Frinak S, Vaupel P, O'Hara MD, et al. Effects of hyperthermia on normal and tumor microenvironment. Radiology 1980;137:523–530. [PubMed: 7433686]
24. Paulides MM, Bakker JF, Neufeld E, van der Zee J, Jansen PP, Levendag PC, et al. Winner of the 'New Investigator Award' at the European Society of Hyperthermia Oncology Meeting 2007. The HYPERcollar: A novel applicator for hyperthermia in the head and neck. Int J Hyperthermia 2007;23:567–576. [PubMed: 18038287]
25. Wu L, McGough RJ, Arabe OA, Samulski TV. An RF phased array applicator designed for hyperthermia breast cancer treatments. Phys Med Biol 2006;51:1–20. [PubMed: 16357427]
26. Fatehi D, van der Zee J, de Bruijne M, Franckena M, van Rhoon GC. RF-power and temperature data analysis of 444 patients with primary cervical cancer: Deep hyperthermia using the Sigma-60 applicator is reproducible. Int J Hyperthermia 2007;23:623–643. [PubMed: 18097850]
27. Weihrauch M, Wust P, Weiser M, Nadobny J, Eisenhardt S, Budach V, et al. Adaptation of antenna profiles for control of MR guided hyperthermia (HT) in a hybrid MR-HT system. Med Phys 2007;34:4717–4725. [PubMed: 18196799]
28. Johnson JE, Neuman DG, Maccarini PF, Juang T, Stauffer PR, Turner P. Evaluation of a dual-arm Archimedean spiral array for microwave hyperthermia. Int J Hyperthermia 2006;22:475–490. [PubMed: 16971368]
29. Juang T, Stauffer PR, Neuman DG, Schlorff JL. Multilayer conformal applicator for microwave heating and brachytherapy treatment of superficial tissue disease. Int J Hyperthermia 2006;22:527–544. [PubMed: 17079212]

30. Boreham DR, Gasmann HC, Mitchel RE. Water bath hyperthermia is a simple therapy for psoriasis and also stimulates skin tanning in response to sunlight. Int J Hyperthermia 1995;11:745–754. [PubMed: 8586897]
31. McNichols RJ, Kangasniemi M, Gowda A, Bankson JA, Price RE, Hazle JD. Technical developments for cerebral thermal treatment: Water-cooled diffusing laser fibre tips and temperature-sensitive MRI using intersecting image planes. Int J Hyperthermia 2004;20:45–56. [PubMed: 14612313]
32. Kangasniemi M, McNichols RJ, Bankson JA, Gowda A, Price RE, Hazle JD. Thermal therapy of canine cerebral tumors using a 980 nm diode laser with MR temperature-sensitive imaging feedback. Lasers Surg Med 2004;35:41–50. [PubMed: 15278927]
33. Tasci TO, Vargel I, Arat A, Guzel E, Korkusuz P, Atalar E. Focused RF hyperthermia using magnetic fluids. Med Phys 2009;36:1906–1912. [PubMed: 19544810]
34. Jordan A, Wust P, Fahling H, John W, Hinz A, Felix R. Inductive heating of ferrimagnetic particles and magnetic fluids: Physical evaluation of their potential for hyperthermia. 1993. Int J Hyperthermia 2009;25:499–511. [PubMed: 19848612]
35. Lynn JG, Zwemer RL, Chick AJ, Miller AE. A new method for the generation and use of focused ultrasound in experimental biology. J Gen Physiol 1942;26:179–193. [PubMed: 19873337]
36. Fry WJ, Barnard JW, Fry EJ, Krumins RF, Brennan JF. Ultrasonic lesions in the mammalian central nervous system. Science 1955;122:517–518.
37. Hynynen K, Darkazanli A, Unger E, Schenck JF. MRI-guided noninvasive ultrasound surgery. Med Phys 1993;20:107–115. [PubMed: 8455489]
38. Ishihara Y, Calderon A, Watanabe H, Okamoto K, Suzuki Y, Kuroda K. A precise and fast temperature mapping using water proton chemical shift. Magn Reson Med 1995;34:814–823. [PubMed: 8598808]
39. Denis de Senneville B, Quesson B, Moonen CT. Magnetic resonance temperature imaging. Int J Hyperthermia 2005;21:515–531. [PubMed: 16147437]
40. Kuroda K, Chung AH, Hynynen K, Jolesz FA. Calibration of water proton chemical shift with temperature for noninvasive temperature imaging during focused ultrasound surgery. J Magn Reson Imaging 1998;8:175–181. [PubMed: 9500277]
41. Cline HE, Hynynen K, Hardy CJ, Watkins RD, Schenck JF, Jolesz FA. MR temperature mapping of focused ultrasound surgery. Magn Reson Med 1994;31:628–636. [PubMed: 8057815]
42. Kennedy JE, ter Haar GR, Cranston D. High intensity focused ultrasound: Surgery of the future? Br J Radiol 2003;76:590–599. [PubMed: 14500272]
43. Arora D, Cooley D, Perry T, Guo J, Richardson A, Moellmer J, et al. MR thermometry-based feedback control of efficacy and safety in minimum-time thermal therapies: Phantom and in vivo evaluations. Int J Hyperthermia 2006;22:29–42. [PubMed: 16423751]
44. Salomir R, Palussiere J, Vimeux FC, de Zwart JA, Quesson B, Gauchet M, et al. Local hyperthermia with MR-guided focused ultrasound: Spiral trajectory of the focal point optimized for temperature uniformity in the target region. J Magn Reson Imaging 2000;12:571–583. [PubMed: 11042639]
45. Salomir R, Vimeux FC, de Zwart JA, Grenier N, Moonen CT. Hyperthermia by MR-guided focused ultra-sound: Accurate temperature control based on fast MRI and a physical model of local energy deposition and heat conduction. Magn Reson Med 2000;43:342–347. [PubMed: 10725875]
46. Vimeux FC, De Zwart JA, Palussiere J, Fawaz R, Delalande C, Canioni P, et al. Real-time control of focused ultrasound heating based on rapid MR thermometry. Invest Radiol 1999;34:190–193. [PubMed: 10084662]
47. Staruch R, Chopra R, Hynynen K. Localised drug release using MRI-controlled focused ultrasound hyperthermia. Int J Hyperthermia 2011;27:156–171. [PubMed: 21158487]
48. Enholm JK, Kohler MO, Quesson B, Mougenot C, Moonen CT, Sokka SD. Improved volumetric MR-HIFU ablation by robust binary feedback control. IEEE Trans Biomed Eng 2010;57:103–113. [PubMed: 19846364]
49. Daum DR, Hynynen K. Thermal dose optimization via temporal switching in ultrasound surgery. IEEE Trans Ultrason Ferroelectr Freq Control 1998;45:208–215. [PubMed: 18244173]

50. Ebbini ES, Cain CA. Multiple-focus ultrasound phased-array pattern synthesis: Optimal driving-signal distributions for hyperthermia. IEEE Trans Ultrason Ferroelectr Freq Control 1989;36:540–548. [PubMed: 18290231]
51. Fan X, Hynynen K. Control of the necrosed tissue volume during noninvasive ultrasound surgery using a 16-element phased array. Med Phys 1995;22:297–306. [PubMed: 7596319]
52. Liu HL, Lin WL, Chen YY. A fast and conformal heating scheme for producing large thermal lesions using a 2D ultrasound phased array. Int J Hyperthermia 2007;23:69–82. [PubMed: 17575725]
53. Dromi S, Frenkel V, Luk A, Traughber B, Angstadt M, Bur M, et al. Pulsed-high intensity focused ultrasound and low temperature-sensitive liposomes for enhanced targeted drug delivery and antitumor effect. Clin Cancer Res 2007;13:2722–2727. [PubMed: 17473205]
54. Patel PR, Luk A, Durrani A, Dromi S, Cuesta J, Angstadt M, et al. In vitro and in vivo evaluations of increased effective beam width for heat deposition using a split focus high intensity ultrasound (HIFU) transducer. Int J Hyperthermia 2008;24:537–549. [PubMed: 18608578]
55. O'Neill BE, Li KC. Augmentation of targeted delivery with pulsed high intensity focused ultrasound. Int J Hyperthermia 2008;24:506–520. [PubMed: 18608574]
56. Negussie AH, Yarmolenko PS, Partanen A, Ranjan A, Jacobs G, Woods D, et al. Formulation and characterisation of magnetic resonance imageable thermally sensitive liposomes for use with magnetic resonance-guided high intensity focused ultrasound. Int J Hyperthermia 2011;27:140–155. [PubMed: 21314334]
57. de Smet M, Heijman E, Langereis S, Hijnen NM, Grull H. Magnetic resonance imaging of high intensity focused ultra-sound mediated drug delivery from temperature-sensitive liposomes: An in vivo proof-of-concept study. J Control Release 2011;150:102–110. [PubMed: 21059375]
58. Yudina A, de Smet M, Lepetit-Coiffe M, Langereis S, Van Ruijssevelt L, Smirnov P, et al. Ultrasound-mediated intra-cellular drug delivery using microbubbles and temperature-sensitive liposomes. J Control Release 2011;155:442–448. [PubMed: 21689699]
59. Guilhon E, Quesson B, Moraud-Gaudry F, de Verneuil H, Canioni P, Salomir R, et al. Image-guided control of transgene expression based on local hyperthermia. Mol Imaging 2003;2:11–17. [PubMed: 12926233]
60. Guilhon E, Voisin P, de Zwart JA, Quesson B, Salomir R, Maurange C, et al. Spatial and temporal control of transgene expression in vivo using a heat-sensitive promoter and MRI-guided focused ultrasound. J Gene Med 200;5:333–342.
61. Hynynen K, Watmough DJ, Mallard JR. Design of ultrasonic transducers for local hyperthermia. Ultrasound Med Biol 1981;7:397–402. [PubMed: 7292784]
62. Cline HE, Schenck JF, Hynynen K, Watkins RD, Souza SP, Jolesz FA. MR-guided focused ultrasound surgery. J Comput Assist Tomogr 1992;16:956–965. [PubMed: 1430448]
63. Hynynen K, Freund WR, Cline HE, Chung AH, Watkins RD, Vetro JP, et al. A clinical, noninvasive, MR imaging-monitored ultrasound surgery method. Radiographics 1996;16:185–195. [PubMed: 10946699]
64. Mougenot C, Quesson B, de Senneville BD, de Oliveira PL, Sprinkhuizen S, Palussiere J, et al. Three-dimensional spatial and temporal temperature control with MR thermometry-guided focused ultrasound (MRgHIFU). Magn Reson Med 2009;61:603–614. [PubMed: 19097249]
65. Partanen A, Mougenot C, Vaara T. Feasibility of agar-silica phantoms in quality assurance of MRgHIFU. AIP Conf Proc 2009;1113:296–300.
66. Ranjan A, Jacobs GC, Woods DL, Negussie AH, Partanen A, Yarmolenko PS, et al. Image-guided drug delivery with magnetic resonance guided high intensity focused ultrasound and temperature sensitive liposomes in a rabbit VX2 tumor model. J Control Release 2012;158:487–94. [PubMed: 22210162]
67. ter Haar G, Shaw A, Pye S, Ward B, Bottomley F, Nolan R, et al. Guidance on reporting ultrasound exposure conditions for bio-effects studies. Ultrasound Med Biol 2011;37:177–183. [PubMed: 21257086]
68. Pennes HH. Analysis of tissue and arterial blood temperatures in the resting human forearm. J Appl Physiol 1948;1:93–122. [PubMed: 18887578]

69. Gasselhuber A, Appanaboyina S, Dreher MR, Partanen A, Wood BJ, Rattay F, et al. Computational modeling of high-intensity focused ultrasound mediated drug delivery. Proc SPIE, 7901:79010F 2011.
70. Tsushima Y, Funabasama S, Aoki J, Sanada S, Endo K. Quantitative perfusion map of malignant liver tumors, created from dynamic computed tomography data. Acad Radiol 2004;11:215–223. [PubMed: 14974597]
71. Sapareto SA, Dewey WC. Thermal dose determination in cancer therapy. Int J Radiat Oncol Biol Phys 1984;10:787–800. [PubMed: 6547421]
72. Hijnen NM, Heijman E, Kohler MO, Ylihautala M, Ehnholm GJ, Simonetti AW, et al. Tumour hyperthermia and ablation in rats using a clinical MR-HIFU system equipped with a dedicated small animal set-up. Int J Hyperthermia 2012;28:141–155. [PubMed: 22335228]
73. Hey S, Ries M, Moonen CT. Online temperature control of focused ultrasound heating using an adaptive PID feedback loop. Proc Intl Soc Mag Reson Med 2011;19:1735.
74. Kim YS, Keserci B, Partanen A, Rhim H, Lim HK, Park MJ, et al. Volumetric MR-HIFU ablation of uterine fibroids: Role of treatment cell size in the improvement of energy efficiency. Eur J Radiol 2011.
75. Voogt MJ, Trillaud H, Kim YS, Mali WP, Barkhausen J, Bartels LW, et al. Volumetric feedback ablation of uterine fibroids using magnetic resonance-guided high intensity focused ultrasound therapy. Eur Radiol 2012;22:411–7. [PubMed: 21901565]
76. Li L, ten Hagen TL, Schipper D, Wijnberg TM, van Rhoon GC, Eggermont AM, et al. Triggered content release from optimized stealth thermosensitive liposomes using mild hyperthermia. J Control Release 2010;143:274–279. [PubMed: 20074595]
77. Lindner LH, Eichhorn ME, Eibl H, Teichert N, Schmitt-Sody M, Issels RD, et al. Novel temperature-sensitive liposomes with prolonged circulation time. Clin Cancer Res 2004;10:2168–2178. [PubMed: 15041738]
78. Yarmolenko PS, Moon EJ, Landon C, Manzoor A, Hochman DW, Viglianti BL, et al. Thresholds for thermal damage to normal tissues: An update. Int J Hyperthermia 2011;27:320–343. [PubMed: 21591897]
79. Jones EL, Oleson JR, Prosnitz LR, Samulski TV, Vujaskovic Z, Yu D, et al. Randomized trial of hyperthermia and radiation for superficial tumors. J Clin Oncol 2005;23:3079–3085. [PubMed: 15860867]
80. Jones E, Thrall D, Dewhirst MW, Vujaskovic Z. Prospective thermal dosimetry: The key to hyperthermia's future. Int J Hyperthermia 2006;22:247–253. [PubMed: 16754346]
81. Thrall DE, LaRue SM, Yu D, Samulski T, Sanders L, Case B, et al. Thermal dose is related to duration of local control in canine sarcomas treated with thermoradiotherapy. Clin Cancer Res 2005;11:5206–5214. [PubMed: 16033838]
82. Oleson JR, Samulski TV, Leopold KA, Clegg ST, Dewhirst MW, Dodge RK, et al. Sensitivity of hyperthermia trial outcomes to temperature and time: Implications for thermal goals of treatment. Int J Radiat Oncol Biol Phys 1993;25:289–297. [PubMed: 8420877]
83. Hand JW, Machin D, Vernon CC, Whaley JB. Analysis of thermal parameters obtained during phase III trials of hyperthermia as an adjunct to radiotherapy in the treatment of breast carcinoma. Int J Hyperthermia 1997;13:343–364. [PubMed: 9278766]
84. Sherar M, Liu FF, Pintilie M, Levin W, Hunt J, Hill R, et al. Relationship between thermal dose and outcome in thermoradiotherapy treatments for superficial recurrences of breast cancer: Data from a phase III trial. Int J Radiat Oncol Biol Phys 1997;39:371–380. [PubMed: 9308941]
85. Lin WL, Roemer RB, Moros EG, Hynynen K. Optimization of temperature distributions in scanned, focused ultrasound hyperthermia. Int J Hyperthermia 1992;8:61–78. [PubMed: 1545164]
86. Lin WL, Chen YY, Lin SY, Yen JY, Shieh MJ, Kuo TS. Optimal configuration of multiple-focused ultrasound transducers for external hyperthermia. Med Phys 1999;26:2007–2016. [PubMed: 10505892]
87. Vigen KK, Daniel BL, Pauly JM, Butts K. Triggered, navigated, multi-baseline method for proton resonance frequency temperature mapping with respiratory motion. Magn Reson Med 2003;50:1003–1010. [PubMed: 14587011]

88. Rieke V, Vigen KK, Sommer G, Daniel BL, Pauly JM, Butts K. Referenceless PRF shift thermometry. Magn Reson Med 2004;51:1223–1231. [PubMed: 15170843]

89. Jenista ER, Galiana G, Branca RT, Yarmolenko PS, Stokes AM, Dewhirst MW, et al. Application of mixed spin iMQCs for temperature and chemical-selective imaging. J Magn Reson 2010;204:208–218. [PubMed: 20303808]

90. El-Sharkawy AM, Schar M, Bottomley PA, Atalar E. Monitoring and correcting spatio-temporal variations of the MR scanner's static magnetic field. MAGMA. 2006;19: 223–236. [PubMed: 17043837]

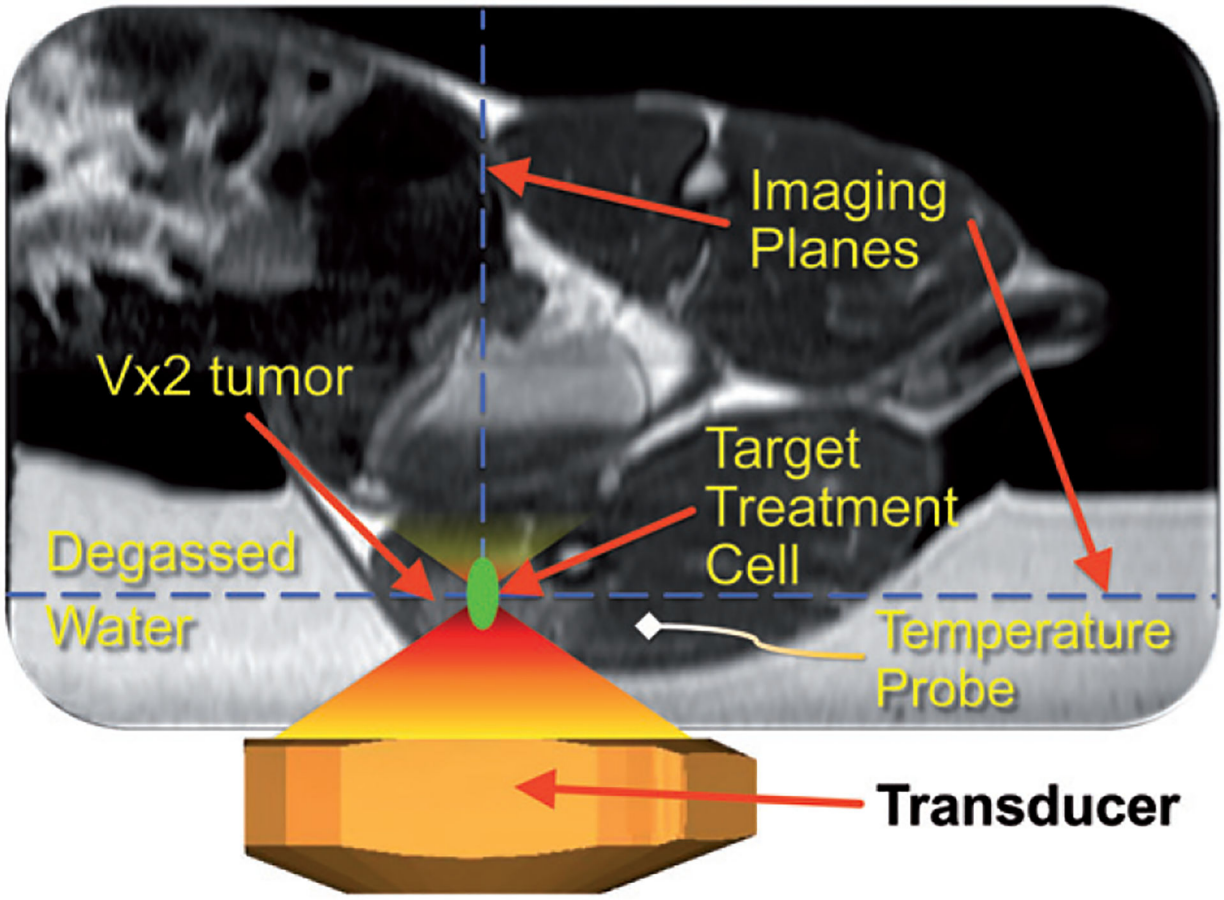

Figure 1.

Schematic of the experimental MR-HIFU hyperthermia set-up, modified from Ranjan et al. [66]. The sagittal imaging plane is shown, with the rabbit in right lateral decubitus position on top of the HIFU platform and the tumour-bearing right hind limb submerged in degassed water. Baseline reference temperature was obtained using a fibre-optic temperature probe inserted in the thigh muscle near the tumour. The imaging slice positions for the thermometry sequence are outlined with a blue dashed line, and the target region within the tumour is shown as a green circle. Depiction of transducer and HIFU beam propagation are meant to be illustrative.

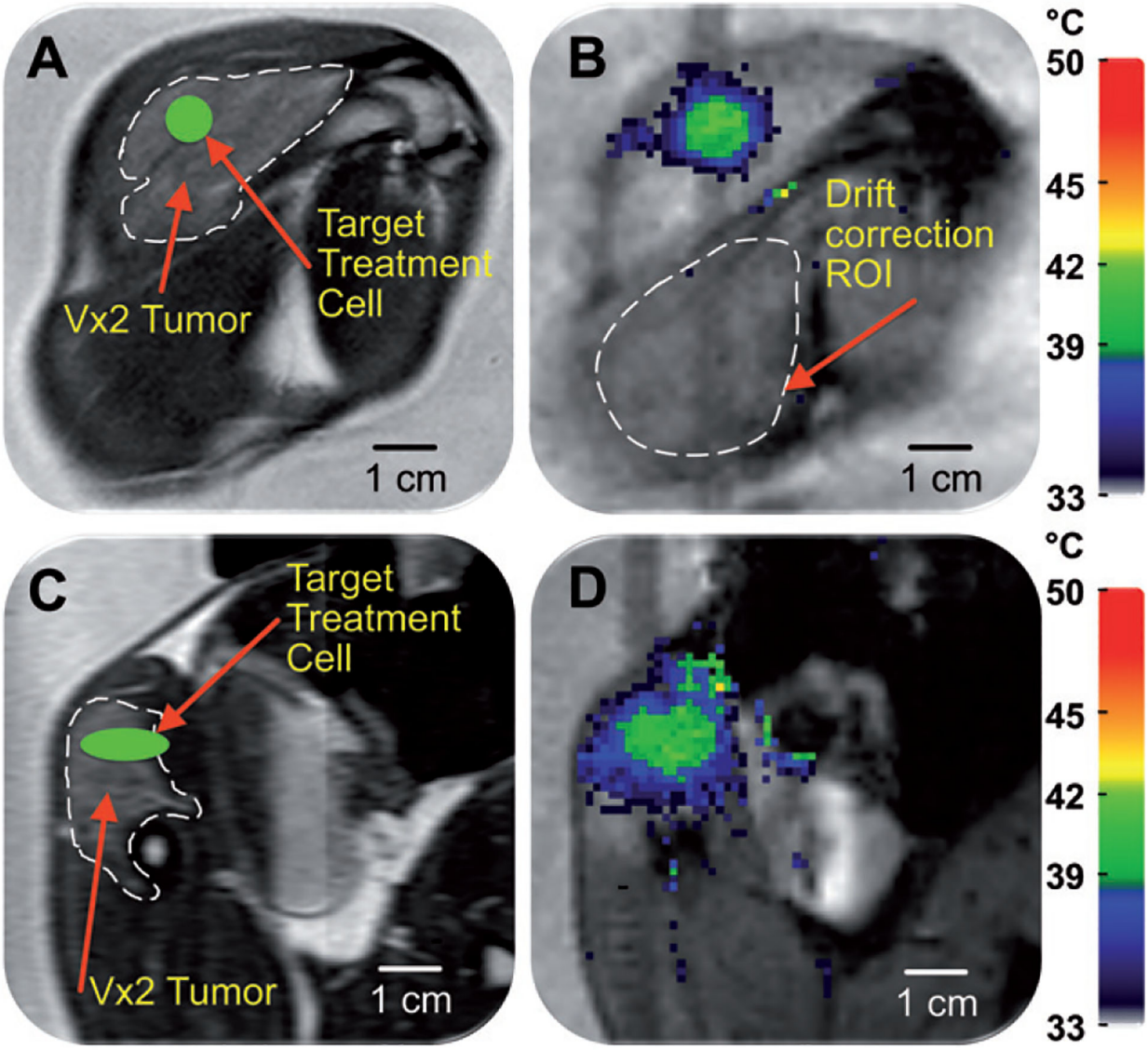

Figure 2.

Planning and temperature mapping for mild hyperthermia: (A) VX2 tumour (hyper-intense) was clearly identified (white dashed line) on the proton density-weighted planning images and a target region within the tumour was chosen (green circle). (B) Temperature maps (colour scale) overlaid on planning images (greyscale) during a mild hyperthermia treatment with an 8 mm treatment cell, showing typical temperature distribution after 5 min of heating. Temperature monitoring and control was achieved in the selected target region with an FFE-EPI imaging sequence, utilising the PRFS method for temperature mapping, and by using the mild hyperthermia feedback control algorithm. The ROI used for magnetic drift correction is outlined with a white dashed line. C and D are the sagittal image planes corresponding to A and B, respectively.

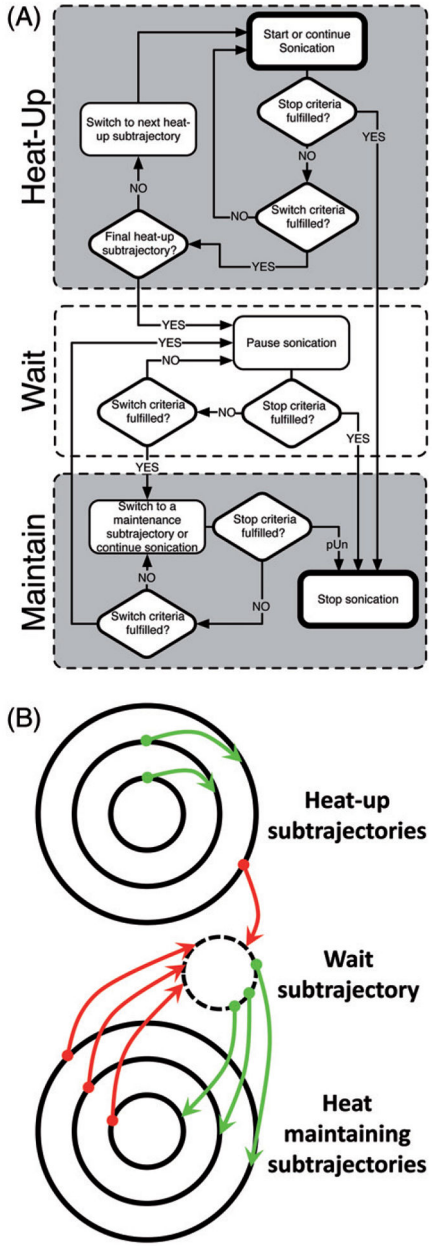

Figure 3.

Mild hyperthermia feedback schematic. (A) During heat-up, sonication cycles through all heat-up trajectories. Once the criteria for every heat-up trajectory are met, heating is paused. When temperature in one of the monitored subtrajectories drops below the lower limit, sonication resumes on that subtrajectory until the upper limit is reached. The cycle of ‘wait’ and ‘maintain’ subtrajectories is repeated until the end of treatment. (B) The schematic demonstrates the flexibility of the binary feedback control algorithm. The algorithm sequentially heats from the innermost to the outermost subtrajectory during heat-up. After the outermost subtrajectory has been heated sufficiently, the algorithm pauses sonication in a ‘wait subtrajectory’. When temperature in one of the subtrajectories decreases below a predefined range, the algorithm is able to heat that subtrajectory specifically.

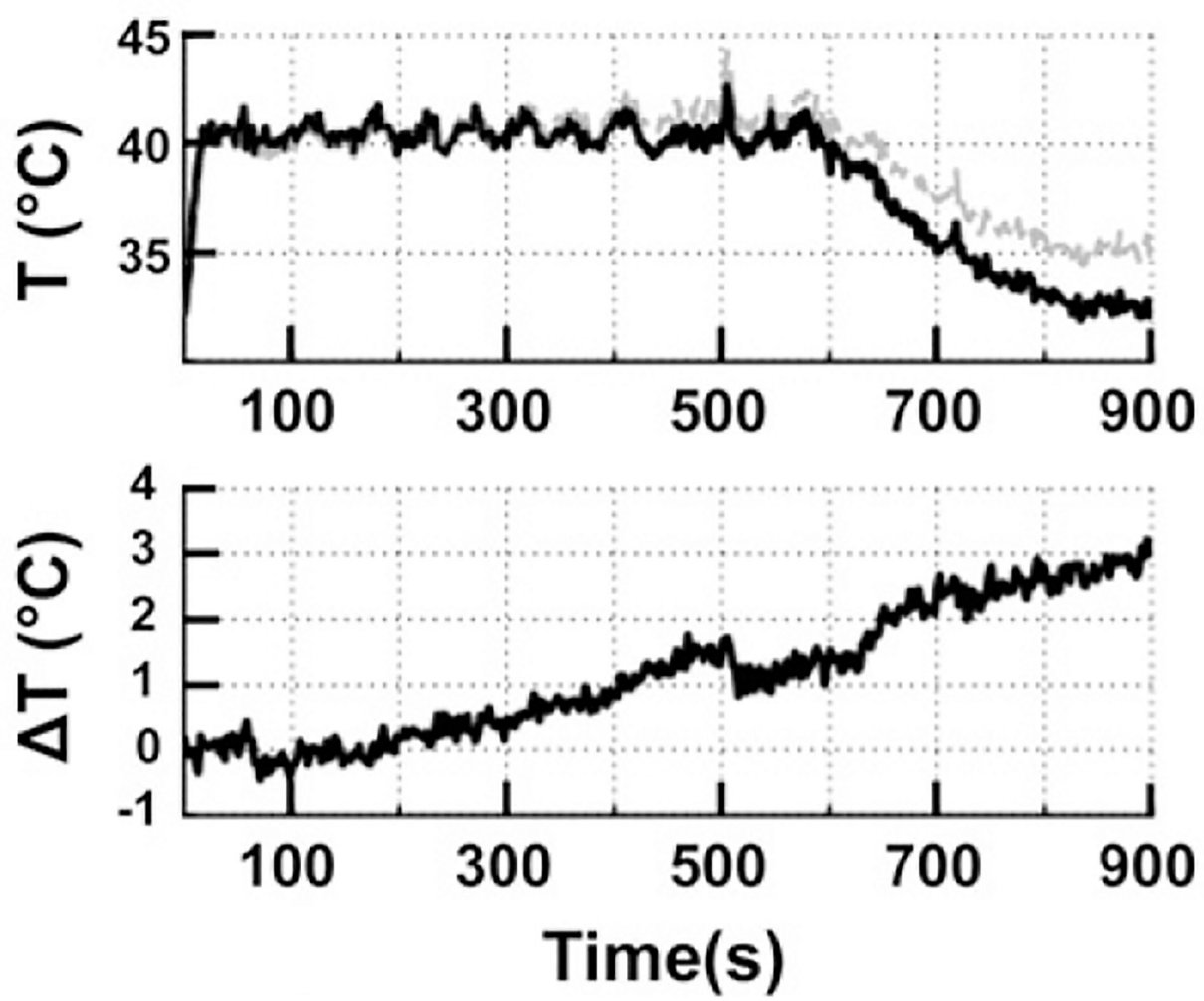

Figure 4.

(A) The mean temperature within an 8mm treatment cell over a 10 min sonication + additional 5 min monitoring in vivo. Uncorrected (grey line) and corrected (black line) temperatures clearly demonstrate the effect of B_0 magnetic field drift. (B) The total baseline temperature drift over 15 min from the same sonication as in A resulted in a change of 3°C.

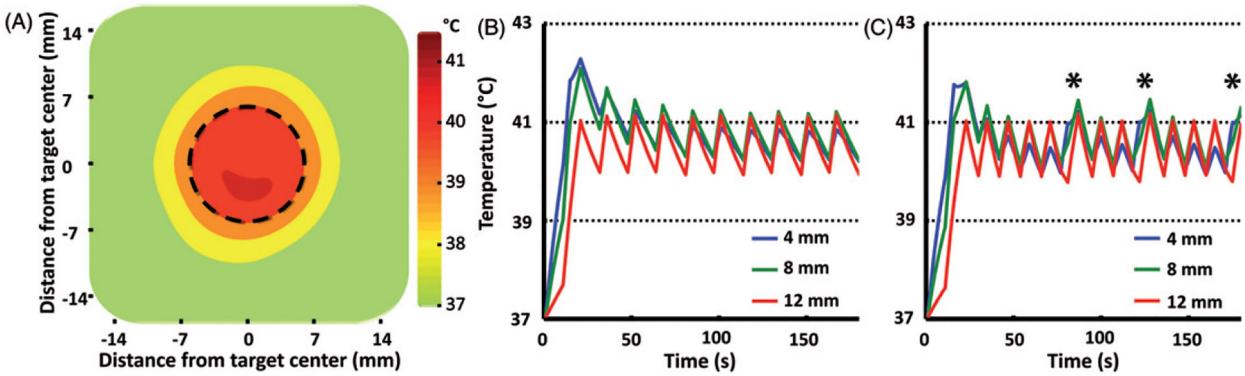

Figure 5.

(A) Time-averaged spatial temperature distribution for a 12mm treatment cell in silico (coronal plane) for 10 min mild hyperthermia with normal perfusion (1 mL/mL/min). Treatment cell is outlined in black dashed line.(B, C) Simulated mean temperature along 4, 8 and 12 mm subtrajectories at two different perfusion levels (B, normal perfusion (1 mL/mL/min) and C, high perfusion (2 mL/mL/min). Only at high perfusion level was it necessary to heat subtrajectories other than 12mm after initial heat-up – notice the heating of the 4mm subtrajectory at 80, 120 and 170 s (marked with asterisks in C).

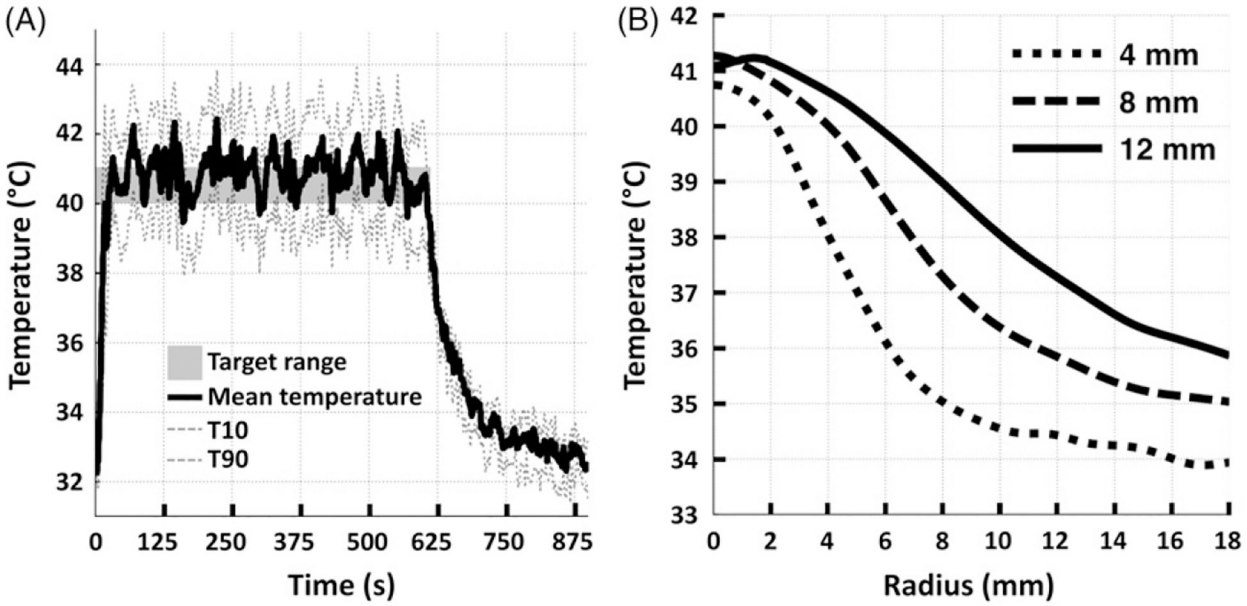

Figure 6.

(A) Representative examples of mean (solid), T10, and T90 (dashed) temperatures within an 8mm treatment cell over a 10 min sonication in vivo. Target temperature range is indicated as a grey box. (B) Representative examples of time-averaged mean temperature radial line profiles centred on the treatment cell for 4 mm, 8mm, and 12 mm treatment cells.

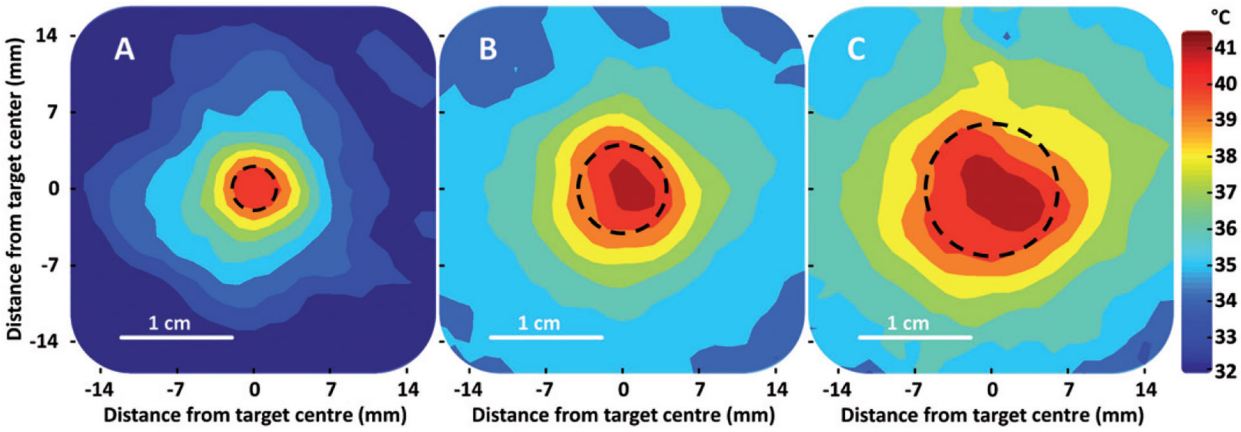

Figure 7.

Representative examples of time-averaged spatial temperature distributions for 4 mm, 8 mm, and 12 mm treatment cells in vivo (coronal plane). The treatment cell is outlined in black dashed line.

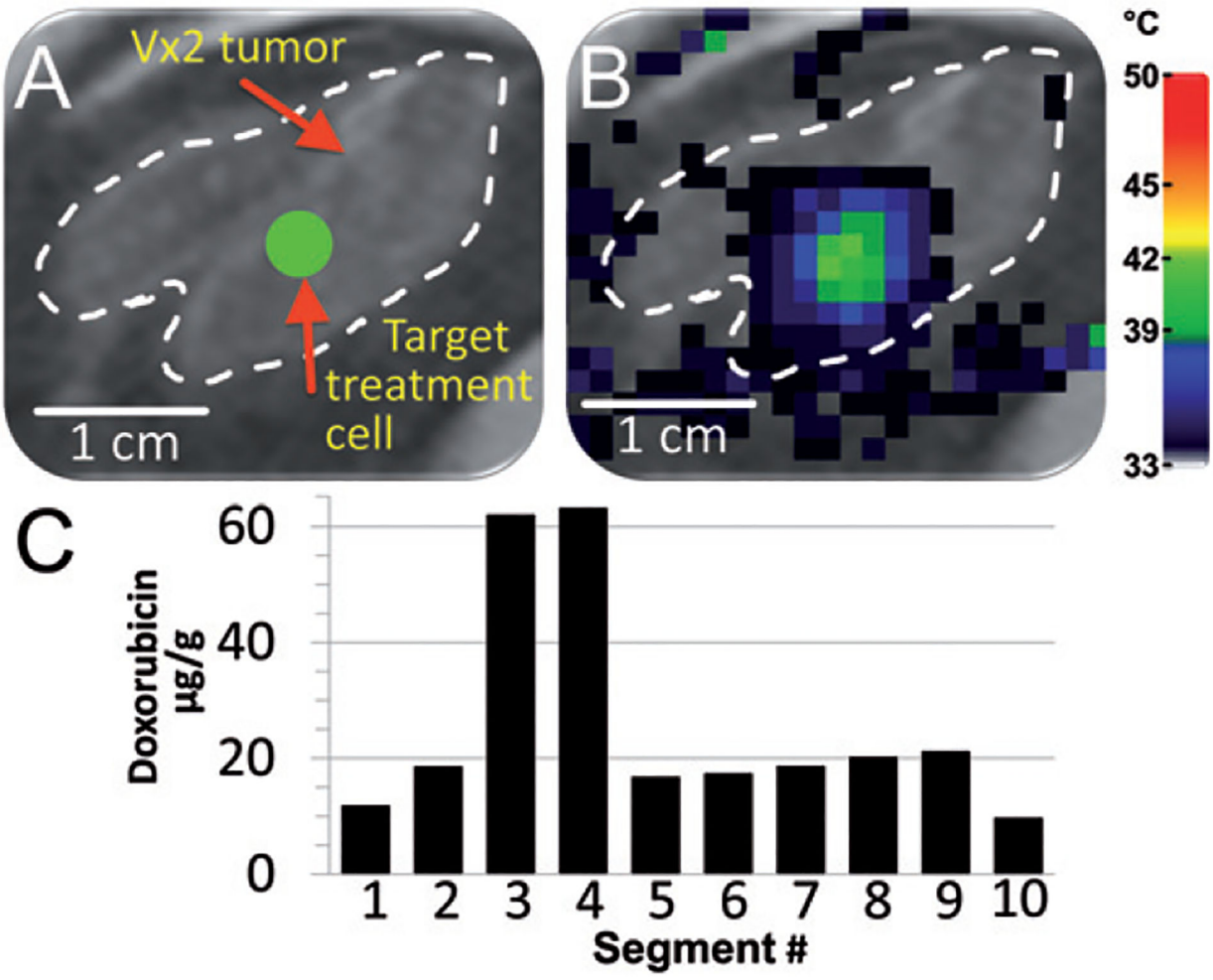

Figure 8.

Demonstration of heterogeneous drug delivery. (A) VX2 tumour was clearly identified (white dashed line) on the proton density-weighted planning images and a target region within the tumour was chosen (green circle). (B) Temperature maps (colour scale) overlaid on planning images (greyscale) during a mild hyperthermia treatment with a 4mm treatment cell, showing typical temperature distribution after 1 min of heating. (C) Doxorubicin concentration in tumour segments was determined by HPLC. Note the higher drug concentration in segments 3 and 4.

Table I.

Summary of the mild hyperthermia sonications performed in vivo and in vitro. Duration of 10 min and a frequency of 1.2 MHz were used for all sonications in vivo. Duration of 30 min and a frequency of 1.2 MHz were used for sonications in vitro. The animal used in the LTSL experiment is identified with an asterisk (⋆).

Rabbit	Reference temperature (°C)	Treatment cell size (mm)	Target tissue	Mean acoustic power and range (W)	Number of sonications	Focal depth from skin (mm)
1	32.7	4.0	Tumour	20.0	2	15
2⋆	33.6	4.0	Tumour	20.0	2	15
3	31.8	4.0	Tumour	23.3 (20–25)	3	12
4	30.8	4.0	Tumour	30	3	18
5	31.0	4.0	Tumour	20	3	10
6	32.2	4.0	Tumour	20	2	14
7	31.1	8.0	Tumour	31.3 (20–35)	4	12
8	32.0	4.0, 8.0, 12.0	Muscle	20, 25, 30	1, 1, 1	15
9	34.8	8.0	Muscle	15	4	15
10	34.5	8.0, 12.0	Tumour	25, 25	4, 3	18
Phantom	35.0	4.0, 8.0, 12.0, 16.0	-	25	8, 4, 4, 4	-

Table II.

Summary of in vitro sonication results. All sonications were performed at a fixed acoustic power of 25 W. The 3D spatial offset was significantly greater than 0 for 4, 8 and 16 mm treatment cells (p=0.0064, p=0.0401 and p=0.0226, respectively, one-sample t-test), but not the 12 mm treatment cell (p=0.0963, one-sample t-test). Target mean temperature range was 40–41°C. All values are mean ± SD.

Treatment cell size (mm)	Number of sonications	Mean (°C)	SD (°C)	T10 (°C)	T90 (°C)	Diameter of area ≥ 40° C (mm)	3D spatial offset (mm)
4.0	8	40.58±0.13	0.72±0.02	41.58±0.05	39.7±0.2	5.0±0.2	0.9±0.6
8.0	4	41.0±0.2	0.76±0.03	41.92±0.11	40.00±0.09	8.8±0.2	1.3±0.7
12.0	4	41.09±0.14	0.71±0.07	41.9±0.2	40.3±0.2	13.3±0.2	1.7±1.4
16.0	4	41.0±0.2	0.86±0.04	42.00±0.09	40.04±0.12	16.2±0.3	2.3±1.1

Table III.

Summary of in vivo sonication results. Target mean temperature range was 40–41°C. The 3D spatial offset was significantly greater than 0 for the 4mm and 8mm treatment cells (p=0.0002 and p=0.0018, respectively, one-sample t-test), but not for the 12mm treatment cell (p=0.1540, one-sample t-test).

Rabbit	Treatment cell size (mm)	Mean (°C)	SD (°C)	T10 (°C)	T90 (°C)	Diameter of area ≥ 40° C (mm)	Mean thermal dose (CEM_{43})	3D spatial offset (mm)
1	4.0	40.7	1.0	41.9	39.4	4.5	1.9	1.2
2	4.0	40.6	1.0	41.9	39.4	4.5	1.7	1.1
3	4.0	40.4	1.1	41.7	39.0	3.8	2.0	1.1
4	4.0	40.8	1.1	42.2	39.4	4.4	2.7	1.6
5	4.0	40.4	1.0	41.7	39.2	4.2	2.2	0.9
6	4.0	40.6	1.1	41.9	39.2	4.2	1.9	0.6
7	8.0	41.0	1.2	42.5	39.4	9.4	5.5	2.1
8	8.0	40.9	1.2	42.4	39.5	9.3	5.9	2.9
9 (loc. 1)	4.0	40.7	1.2	42.2	39.2	4.5	1.0	1.7
9 (loc. 2)	8.0	41.3	1.4	43.0	39.5	9.1	3.2	1.9
9 (loc. 3)	12.0	41.2	1.5	43.7	39.6	11.6	6.1	4.8
10 (loc. 1)	8.0	40.7	1.1	42.1	39.3	8.1	4.5	2.5
10 (loc. 2)	12.0	40.6	1.1	41.9	39.2	11.47	3.1	2.9

Loc., location

Table IV.

Summary of sonication duration in different subtrajectories (as percentages of total treatment time), sonication energies, and sonication efficiencies in vivo. Energies and efficiencies are reported as mean ± SD.

Rabbit	Treatment cell size(mm)	Target tissue	Sonication on (%)	4 mm subtr.(%)	8 mm subtr.(%)	12 mm subtr.(%)	Wait subtr.(%)	Energy (kJ)	Efficiency(cm^3/MJ)
1	4.0	Tumour	70	70	-	-	30	4.4±0.4	24±0.8
2	4.0	Tumour	60	60	-	-	40	3.7±0.4	30±5.2
3	4.0	Tumour	85	85	-	-	15	6.2±0.2	14±1.7
4	4.0	Tumour	55	55	-	-	45	5.7±0.6	11±1.9
5	4.0	Tumour	70	70	-	-	30	5.1±0.7	14±5.1
6	4.0	Tumour	65	65	-	-	35	4.4±1.5	29±8.3
7	8.0	Tumour	71	6	65	-	29	7.1±0.4	80±5.0
8	4.0	Muscle	39	39	-	-	61	2.5	30
8	8.0	Muscle	52	4	48	-	48	4.5	110
8	12.0	Muscle	53	11	4	38	47	5.6	250
9	8.0	Muscle	64	3	61	-	36	3.1±0.4	160±20.0
10	8.0	Tumour	67	4	63	-	33	5.5±0.4	80±8.4
10	12.0	Tumour	79	12	4	63	21	6.9±0.3	180±7.7

Subtr., subtrajectory.